ORIGINAL PAPER

Propeller-rotor aerodynamic interaction in helicopter air-to-air refueling: an analytical solution for rotor trim, including a sensitivity study

Berend G. van der Wall[1] (ID)

Abstract
During helicopter air-to-air refueling the rotor of the helicopter might enter the slipstream of the tanker aircraft's propeller. Based on blade element momentum theory, the impact of this jet on rotor blade aerodynamics is formulated. Rotor controls required to re-trim are solved analytically and verified by numerical solution of the problem. The collective and cyclic controls needed for disturbance rejection are computed for a typical air-to-air refueling scenario. A propeller wake affecting the retreating side of the rotor requires much more pilot controls to retrim than an impingement on the advancing side. Variations of rotor angle of attack, propeller radius, propeller thrust and rotor thrust are performed.

Keywords Helicopter · Helicopter rotor · Interactional aerodynamics · Propeller-rotor interaction · Helicopter air-to-air refueling · Blade element theory

Abbreviations

AAR	Air-to-air refueling
F(AI)²R	Future air-to-air refueling (DLR project)
HAAR	Helicopter air-to-air refueling

List of symbols

a_{ij}	System matrix elements
A, B	System, excitation matrix
b_{ij}	Excitation matrix elements
a_∞	Speed of sound, m/s
c	Rotor blade chord, m
c_μ	Advance ratio term, $c_\mu = 2\mu_0 + \Delta\mu$
$C_{l\alpha}$	Lift curve slope
C_{Mx}	Aerodynamic rolling moment, $C_{Mx} = M_x/\left(\rho\pi R^2(\Omega R)^2 R\right)$
C_{My}	Aerodynamic pitching moment, $C_{My} = M_y/\left(\rho\pi R^2(\Omega R)^2 R\right)$
C_T	Rotor thrust coefficient, $C_T = T/\left(\rho\pi R^2(\Omega R)^2\right)$
dL	Non-dimensional blade element lift, $dL = \frac{\rho}{2}(\Omega R)^2 U_T^2 c C_{l\alpha}\alpha\, dy/\left(\rho\pi R^2(\Omega R)^2\right)$
dC_T	Blade element contribution to the thrust coefficient, $dC_T = N_b dL$

✉ Berend G. van der Wall
  berend.vanderwall@dlr.de

1   German Aerospace Center (DLR), Lilienthalplatz 7,
    38108 Braunschweig, Germany

D_∞	Contracted slipstream diameter, m
g	Gravitational constant, $g = 9.81$ m/s²
h	Height above sea level, m
m	Vehicle mass, kg
M	Mach number, $M = V/a_\infty$
N_R	Number of rotors
N_b	Number of blades
r	Non-dimensional radial coordinate
R	Rotor or slipstream radius, m
$\vec{u}$	Excitation vector
U_T	Non-dimensional tangential velocity, referenced to ΩR
U_P	Non-dimensional perpendicular velocity, referenced to ΩR
u, V	Velocity, m/s
x, y	Non-dimensional rotor longitudinal, lateral coordinate
α	Angle of attack, deg
Δ	Perturbation
$\Delta_{\mu\lambda}$	Mixed term of advance ratio and inflow perturbations, $\Delta_{\mu\lambda} = \mu_0\Delta\lambda + \lambda\Delta\mu$
ϵ	Glide ratio
Θ	Blade element pitch angle, deg
λ	Total inflow ratio, $\lambda = \lambda_i + \mu_z$
λ_C	Propeller axial inflow ratio, $\lambda_C = V_\infty/(\Omega R)_p$
λ_i	Induced inflow ratio, $\lambda_i = v_i/(\Omega R)$
μ_∞	Flight speed ratio, $\mu_\infty = V_\infty/(\Omega R)$

μ	Advance ratio, $\mu = \mu_\infty \cos\alpha_S$
μ_z	Inflow ratio, $\mu_z = -\mu_\infty \sin\alpha_S$
ρ	Air density, kg/m^3
σ	Rotor solidity, $\sigma = N_b c/(\pi R)$
ψ	Azimuth angle, deg
Ω	Rotor rotational speed, rad/s

Subscripts

$airc, hel$	Aircraft, helicopter
beg, end	Begin and end of azimuth region
C, S	Cosine, sine component
i	Induced
NE	Never exceed
p	Propeller
S	Rotor shaft
tip	Blade tip
tw	Blade twist
up, low	Upper and lower radial integration bound
z	Z-direction
0	Undisturbed rotor trim value
$1, 2$	Left and right end of slipstream
75	At 75% radius
∞	Values of the operational condition

1 Introduction

Air-to-air refueling (AAR) of aircraft is mainly used in military operations to extend the range of aircraft, reduce ground exposure and hence, save time. Helicopter AAR (=HAAR) can also be critical for Search and Rescue missions, especially for those on the ocean far from the mainland. It requires a tanker aircraft, usually with hoses on either side of the wing outside of the propellers, but inside the wing tips. A first HAAR demonstration was reported in 1966, where a C-130 tanker aircraft was used for refueling a HH-3C helicopter, Ref. [1].

Due to the comparably low maximum speed of helicopters during HAAR, the tanker aircraft has to fly close to its minimum speed and at low altitude, leaving little margin for the helicopter to its never-exceed speed V_{NE}, and also little margin for the tanker aircraft before reaching its minimum speed. This implies the tanker flying with less than its maximum take-off mass, at low altitude (for high air density), with deflected flaps (increasing the wing surface and introducing large camber, both for maximum lift capability), and with high propeller thrust (to overcome the aircraft drag in this situation).

Helicopters, therefore, have to get into and sustain position within an area of large disturbances generated by the aircraft, such as the general wing downwash, strong tip vortices from both the wing and either ends of the deflected flaps, eventually separated flow turbulences, and the jet within the slipstream of the propellers. This condition comes along with a high level of rotor power and large collective and longitudinal cyclic control angles (Θ_{75}, Θ_S) for helicopter trim. Although many publications exist on operational aspects such as handling qualities and control laws, e.g. Ref. [2], the discussion of individual physical phenomena acting at the helicopter rotor were so far limited to the downwash and vortex problems (which also affect the drogue motion). An excellent overview of AAR aspects and extensive literature is given in Ref. [3], but mentioning HAAR only in respect to "*if commercial uses for autonomous search and rescue and other naval activities become viable there may be a desire to have an autonomous helicopter refuelling mechanism which, as is evident by piloted HAAR, comes with its own challenges and specific procedures*".

For trials to be executed in motion-based simulators, Ref. [4], computational fluid dynamics computations were performed at DLR using a model of an A400M-like aircraft configuration with actuator disks representing the propellers, Ref. [5]. The velocities within the volume all around the trimmed aircraft were computed in advance and used within the simulator. Trials in the simulator were executed within the "Future Air-to-Air Refueling" [F(AI)^{2}R] project of DLR "*to eventually develop methods and systems for the automation of the aerial refueling process (including pilot assistance), for fixed wing and rotary wing aircraft,*" Ref. [5]. This project partly investigated HAAR in DLR's motion-based simulator AVES, which required the introduction of a realistic flow field environment before focusing on handling qualities, pilot assistance and improved procedures.

Problems encountered during HAAR tests with the A400M, Ref. [6], that later were solved by a longer hose than originally planned, underlined the need for a HAAR simulator tool of high fidelity. Investigations regarding HAAR conducted during the F(AI)^{2}R project did not look deeper into the physics acting within the helicopter rotor, rather to the overall reaction and control of a CH53-like helicopter within the tanker aircraft's flow field. The impact of vortices (from wing tips or flap ends) on rotor trim controls, blade flapping, and rotor power were analytically solved in former publications, e.g. Ref. [7].

The work of Ref. [4] conducted during the F(AI)^{2}R project, however, provided some flow field data in the propeller wake, and exemplarily the inner propeller's induced velocities are shown in a slice through its slipstream in Fig. 1. Operational conditions are an aircraft mass of 13 t with an attitude of 11.65 deg. Below the horizontal stabilizer the slipstream velocities still reach values of up to ca. $\Delta V_x = 35$ m/s relative to of $V_\infty = 65.7$ m/s.

The big propellers of the tanker aircraft obviously generate a stream tube with accelerated air velocity due to their high thrust. A helicopter rotor partially or fully immersed in this propeller jet experiences aerodynamic disturbances that
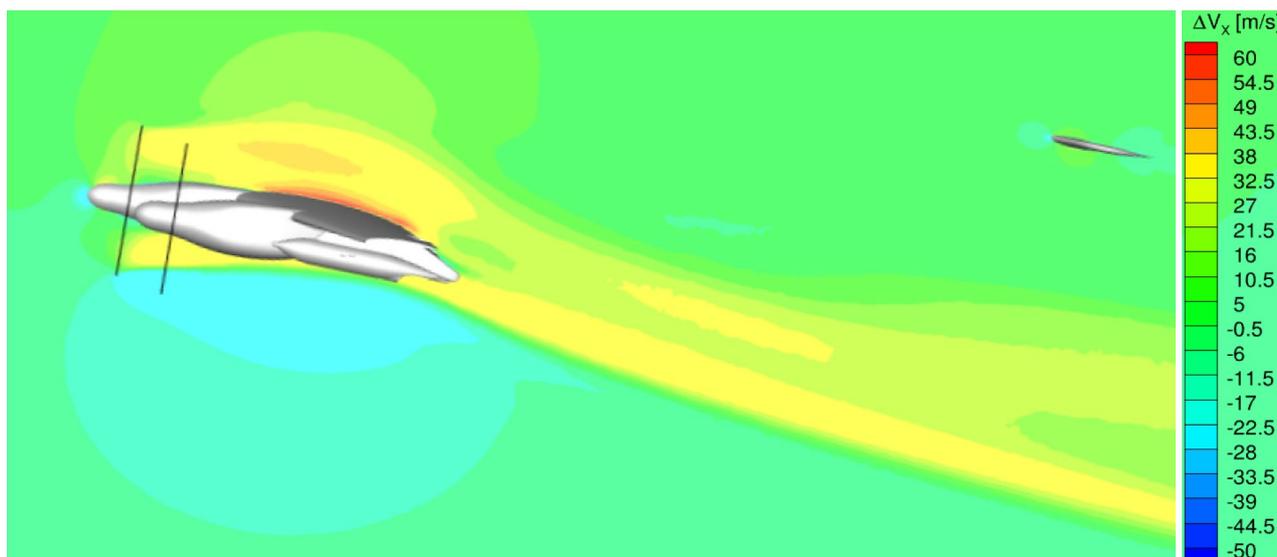
Source: P.Löchert

Fig. 1 Horizontal velocities induced by the aircraft wing and the propeller slipstream. $V_\infty = 65.7$ m/s, $h = 2130$ m. *Source*: P. Löchert

need to be rejected by pilot controls. As an example used here, a tanker aircraft of the size of an A400M and a transport helicopter of the size of a CH-53G as used within the F(AI)²R project are taken with their characteristic parameters given in Table 1. The fundamental problem is sketched in Fig. 2, using the geometric properties of Table 1. To simplify the problem the following assumptions are made: aircraft and helicopter are flying at the same speed, the propeller and rotor centers are at the same height (which represents the worst-case scenario), the propeller slipstream is fully contracted (i.e., the horizontal separation of propeller and helicopter rotor is sufficiently large). The helicopter rotor is inclined nose-down because the rotor thrust has to carry the helicopter weight and also to overcome its drag at this high speed.

The propeller has a diameter roughly half of the rotor radius, therefore, almost half of the rotor radius is exposed to an increased velocity relative to the free airstream. Assuming both aircraft are flying at $V_\infty = 65.7$ m/s the helicopter would have a speed margin of only 1 m/s to its maximum cruising speed and about 16 m/s to its $V_{NE} = 82$ m/s, which usually is only obtained in dive conditions. In the upper part of Fig. 2 (a), the propeller slipstream only affects the advancing side of the rotor, locally increasing the advance ratio (and with it the Mach numbers and compressibility effects) in a lateral strip extending from y_1 to y_2.

Additionally, a configuration with the slipstream on the retreating side is sketched in Fig. 2 (a), where the additional velocity causes an increased area of reversed flow (shaded in light grey, extending the radial range from $r = \mu$ to $\mu + \Delta\mu$ at $\psi = 270$ deg) and in the rest of the area affected

Table 1 Technical data of tanker aircraft and transport helicopter

| Tanker aircraft		Transport helicopter	
Parameter, symbol, unit	Value	Parameter, symbol, unit	Value
Max. take-off mass, -, t	141	Max. take-off mass, -, t	19.5
Minimum speed, V_{min}, m/s	63.9[*]	Maximum cruise speed, V_{max}, m/s	66.7
		Never exceed speed, V_{NE}, m/s	82.0
Number of propellers, N_p, -	4	Number of rotors, N_R, -	1
Number or propeller blades, N_{bp}, -	8	Number of rotor blades, N_b, -	6
Propeller radius, R_p, m	2.67	Rotor radius, R, m	11
Blade chord length, c_p, m	0.5[*]	Blade chord length, c, m	0.74
Propeller solidity, σ_p, -	0.477[*]	Rotor solidity, σ, -	0.128
Propeller tilt angle, $\Delta\alpha_p$, deg	− 2	Blade twist, Θ_{tw}, deg/R	− 6.0

[*]estimated
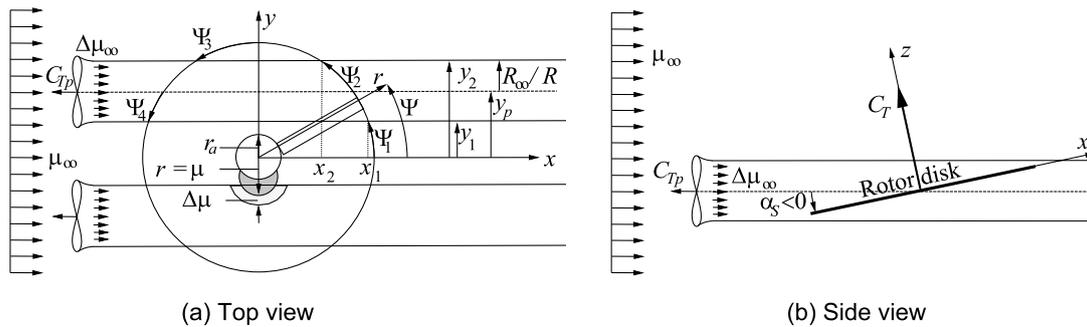
Fig. 2 Sketch of a rotor immersed in the stream tubes of two propellers

by it, reduces the effective velocity acting at the blade, thus reducing its maximum lifting capability. In the side view, Fig. 2 (b), it is seen that in this configuration the entire rotor disk will be immersed inside the propeller slipstream.

The interaction of the propeller slipstream with the helicopter rotor and the controls required to reject the disturbance were solved analytically for the first time on Ref. [8]. The subject of this article is to validate Ref. [8] by a numerical solution and to perform a sensitivity study with respect to the rotor shaft angle, the propeller slipstream diameter, its velocity, and the rotor thrust. The analysis of the problem is outlined first, followed by the trim of the undisturbed rotor as the reference condition, and succeeded by the sensitivity study.

2 Problem analysis

2.1 Approach

The propeller-induced velocity v_{ip} at the considered flight speed (aerodynamically equivalent to a rotor in axial climb) needs to be evaluated, based on momentum theory as outlined in the classical literature. Aerodynamically, the propeller can be treated in the same manner as a rotor in axial climb. For the investigation performed here the propeller

is considered as an actuator disk and the helicopter rotor is considered having rigid, pre-twisted blades with the blade pitch angle as sole degree of freedom, because the focus here is on the aerodynamic aspect of trim disturbance and the disturbance rejection.

First, the propeller's thrust T_p must be estimated by means of Eq. (1), and this can roughly be based on the aircraft's mass m_{airc}, its glide ratio ϵ, and the number of propellers N_p. Then, the induced velocity v_{hp} for static thrust at zero flight speed (equivalent to a helicopter in hover) and the associated induced inflow ratio λ_{hp} of that thrust can be computed, with R_p as the propeller radius and Ω_p its rotational frequency, see Eq. (1). Therein, g is the gravitational constant, and ρ the air density.

$$T_p \approx \frac{m_{airc}g}{\epsilon N_p}; \quad v_{hp} = \sqrt{\frac{T_p}{2\rho\pi R_p^2}}; \quad \lambda_{hp} = \frac{v_{hp}}{\Omega_p R_p} \tag{1}$$

Next, based on the axial inflow ratio λ_C of the propeller at the flight speed V_∞ of the tanker aircraft, the induced velocity v_{ip} in the propeller's disk at the speed of flight is resulting. The helicopter rotor, due to its large distance to the propeller, is subjected to the fully developed slipstream of the propeller, which has twice the induced velocity than within the propeller disk, leading to a perturbation tip speed ratio $\Delta\mu_\infty$. Following momentum theory, finally the perturbation advance ratio $\Delta\mu$ in the helicopter rotor disk and the perturbation inflow radio $\Delta\mu_z$ normal to the disk can be computed. All these are given in Eq. (2).

$$\lambda_C = \frac{V_\infty}{\Omega_p R_p}; \qquad \overline{\lambda_C} = \frac{\lambda_C}{2\lambda_{hp}}; \qquad \lambda_{ip} \approx \lambda_{hp}\left(\sqrt{\overline{\lambda_C}^2 + 1} - \overline{\lambda_C}\right)$$

$$\Delta V_\infty = 2\lambda_{ip}\Omega_p R_p; \qquad \Delta\mu_\infty = \frac{\Delta V_\infty}{\Omega R}; \qquad \Delta\mu = \Delta\mu_\infty \cos\alpha_S; \qquad \Delta\mu_z = -\Delta\mu_\infty \sin\alpha_S \tag{2}$$

In the worst case, the full slipstream diameter enters the rotor disk. This requires to compute the propeller slipstream contraction radius R_∞ that can be estimated by Eq. (3), using momentum theory, Ref. [10]. D_∞ is the contracted slipstream diameter.

$$\frac{R_\infty}{R_p} = \sqrt{\frac{\overline{\lambda_C} + \sqrt{\overline{\lambda_C}^2 + 1}}{2\sqrt{\overline{\lambda_C}^2 + 1}}}; \qquad y_2 - y_1 = \frac{2R_\infty}{R} = \frac{D_\infty}{R} \quad (3)$$

of rotation, and the component perpendicular to it. In non-dimensional form (all velocities are divided by the tip speed ΩR), these are U_T and U_P, respectively, Eq. (5). With the simplifying assumption of no flapping motion, the perpendicular component U_P is identical to the total inflow $\lambda = \lambda_0 + \Delta\lambda$, where both components consist of the inflow μ_z due to forward speed and rotor angle of attack α_S, and the induced inflow due to thrust, λ_i. Using the small angle assumption, the angle of attack α at a blade element can be computed from the local pitch angle and the velocity components, see Eq. (5).

$$U_T = (r + \mu_0 \sin\psi) + (\Delta\mu \sin\psi) = U_{T0} + \Delta U_T$$
$$U_P = \underbrace{(\mu_{z0} + \lambda_{i0})}_{\lambda_0} + \underbrace{(\Delta\mu_z + \Delta\lambda_i)}_{\Delta\lambda} = U_{P0} + \Delta U_P$$

$$\Theta = \underbrace{\left[\Theta_{tw}(r - 0.75) + \Theta_{75} + \Theta_S \sin\psi + \Theta_C \cos\psi\right]}_{\Theta_0} + \underbrace{\left(\Delta\Theta_{75} + \Delta\Theta_S \sin\psi + \Delta\Theta_C \cos\psi\right)}_{\Delta\Theta} \quad (5)$$

$$= \Theta_0 + \Delta\Theta$$

$$\alpha = \Theta - \arctan\frac{U_P}{U_T} \approx \Theta_0 + \Delta\Theta - \frac{U_{P0} + \Delta U_P}{U_{T0} + \Delta U_T}$$

Due to the nose-down disk tilt angle α_S in this fast forward flight condition as sketched in Fig. 2 (b), the flight speed ratio μ_∞ must be decomposed into its in-plane contribution, the advance ratio μ_0, and the inflow ratio normal to the disk, μ_{z0}. In the region occupied by the propeller slipstream, both components get additional contributions from the slipstream velocity, $\Delta\mu$ and $\Delta\mu_z$, which are zero outside of it, Eq. (4).

$$\begin{aligned} \mu &= \mu_0 + \Delta\mu; & \mu_0 &= \mu_\infty \cos\alpha_S \\ \mu_z &= \mu_{z0} + \Delta\mu_z; & \mu_{z0} &= -\mu_\infty \sin\alpha_S \\ \Delta\mu &= \Delta\mu_z = 0 & \left.\right\} &\; -1 \leq y \leq y_1 \vee y_2 \leq y \leq 1 \\ \Delta\mu &= \Delta\mu_\infty \cos\alpha_S & \left.\right\} &\\ \Delta\mu_z &= -\Delta\mu_\infty \sin\alpha_S & \left.\right\} &\; y_1 < y < y_2 \end{aligned} \quad (4)$$

$\Delta\mu$ in the region occupied by the propeller slipstream significantly increases the local advance ratio. For computation of the helicopter rotor section airloads the local angle of attack α must be known, which requires the blade pitch angle Θ (consisting of the linear pre-twist angle Θ_{tw}, the collective control angle at 75% radius Θ_{75} and the cyclic control angles Θ_S and Θ_C), the velocity component acting tangential to the blade element in the plane

Therein, the perturbations of control angles ($\Delta\Theta_{75}, \Delta\Theta_S, \Delta\Theta_C$) are used to reject the propeller disturbances in rotor thrust and hub moments in order to keep the trim constant. Because the induced inflow ratio λ_i of the rotor depends on the advance ratio and the thrust coefficient, it will be different in the unaffected part of the rotor disk and in the region occupied by the propeller slipstream. Assuming a small rotor disk tilt angle, the inflow ratio of the unaffected rotor can be estimated based on momentum theory in forward flight, Ref. [9], and is given by Eq. (6).

$$\lambda_i \approx \frac{\lambda_h^2}{\mu} = \frac{C_T/2}{\mu_0 + \Delta\mu} = \underbrace{\frac{C_T}{2\mu_0}}_{\lambda_{io}} \underbrace{- \frac{C_T}{2\mu_0}\frac{\Delta\mu}{\mu_0 + \Delta\mu}}_{\Delta\lambda_i} = \lambda_{io} + \Delta\lambda_i$$

(6)

The first term represents the induced inflow in the undisturbed rotor area and the second term represents the difference to it applied only in the region occupied by the propeller slipstream. Because $\Delta\lambda_i < 0$, the induced inflow ratio in the region occupied by the slipstream is less than in the undisturbed rotor due to the increased advance ratio. The nondimensional (divided by $\rho\pi R^2(\Omega R)^2$) section

lift dL of a unit span dr and the nondimensional aerodynamic moment rdL about the hub center are computed by means of blade element momentum theory with the usual assumptions, i.e. linear, incompressible, steady 2D aerodynamics, constant inflow, and small angle assumption. The contribution of all N_b rotor blades to the rotor thrust coefficient C_T introduces the rotor's solidity $\sigma = N_b c/(\pi R)$, Eq. (7).

$$dL = \frac{(\rho/2)\left(\Omega R U_T\right)^2 c C_{l\alpha}\alpha dy}{\rho(\Omega R)^2 \pi R^2} \approx \frac{c}{\pi R}\frac{C_{l\alpha}}{2}U_T^2\left[\Theta - \frac{U_P}{U_T}\right]dr$$

$$dC_T = N_b dL = \frac{\sigma C_{l\alpha}}{2}\left[U_T^2\Theta - U_T U_P\right]dr \tag{7}$$

Again, this can be split into the component of the undisturbed rotor and of the disturbance, Eq. (8).

$$dC_T = dC_{T0} + \Delta dC_T$$

$$dC_{T0} = \frac{\sigma C_{l\alpha}}{2}\left[U_{T0}^2\Theta_0 - U_{T0}U_{P0}\right]dr \tag{8}$$

$$\Delta dC_T = \frac{\sigma C_{l\alpha}}{2}\left[\underbrace{U_T^2\Delta\Theta}_{[1],[2]} + \underbrace{\left(2U_{T0}\Delta U_T + \Delta U_T^2\right)\Theta_0}_{[3]} + \underbrace{\left(-U_T\Delta U_P - \Delta U_T U_{P0}\right)}_{[4]}\right]dr$$

Therein, [1] denotes the component $U_{T0}^2\Delta\Theta$ acting on the entire disk, while all other components are only acting in the part of the disk occupied by the slipstream, because ΔU_T and ΔU_P are zero outside of it: [2] denotes the component $\left(2U_{T0}\Delta U_T + \Delta U_T^2\right)\Delta\Theta$, [3] the contribution of the blade twist and trim control angles, and [4] the mixed terms of advance ratio and inflow ratio perturbations.

2.2 Rotor trim in undisturbed air

The control angles for trimming the undisturbed rotor are required before solving for the additional control angles required for disturbance rejection. The mean thrust coefficient of the undisturbed rotor is obtained by time average over one revolution and integrating from 0 to 1 in radial direction (ignoring root cutout and tip losses for simplicity), Eq. (9). This results in a set of three linearly coupled algebraic equations to solve for the trim control angles: collective, longitudinal cyclic and lateral cyclic. Using the rotor coordinate system as given in Fig. 2 (a), the contributions to the hub moments are $dC_{Mx} = rdL\sin\psi$ and $C_{My} = -rdL\cos\psi$.

$$\left\{\begin{array}{c} C_T \\ C_{Mx} \\ C_{My} \end{array}\right\} = \frac{1}{2\pi}\int_0^{2\pi}\int_0^1\left\{\begin{array}{c} 1 \\ r\sin\psi \\ -r\cos\psi \end{array}\right\}dC_{T0}\,d\psi \tag{9}$$

Evaluation of the integrals using dC_{T0} from Eq. (8) and velocities from Eq. (5) results in Eq. (10):

$$\left\{\begin{array}{c} C_T \\ C_{Mx} \\ C_{My} \end{array}\right\} = \frac{\sigma C_{l\alpha}}{2}\left\{\begin{array}{c} \left(\frac{1}{3} + \frac{\mu_0^2}{2}\right)\Theta_{75} + \frac{\mu_0}{2}\Theta_S - \frac{\mu_0^2}{8}\Theta_{tw} - \frac{1}{2}\lambda_0 \\ \frac{\mu_0}{3}\Theta_{75} + \left(\frac{1}{8} + \frac{3\mu_0^2}{16}\right)\Theta_S - \frac{\mu_0}{4}\lambda_0 \\ -\left(\frac{1}{8} + \frac{\mu_0^2}{16}\right)\Theta_C \end{array}\right\} \tag{10}$$

The third row immediately can be solved for Θ_C, because it is not coupled with the first two equations. For $C_{My} = 0$ it follows that $\Theta_C = 0$, due to the symmetry of flow conditions about the y-axis. From the first two equations, the collective and longitudinal cyclic control angles can be computed. These two equations can formally be written as Eq. (11)

$$\begin{bmatrix} a_{11} & a_{12} \\ a_{21} & a_{22} \end{bmatrix}\left\{\begin{array}{c} \Theta_{75} \\ \Theta_S \end{array}\right\} = \left\{\begin{array}{c} b_1 \\ b_2 \end{array}\right\} \quad\Rightarrow\quad \left\{\begin{array}{c} \Theta_{75} \\ \Theta_S \end{array}\right\}$$
$$= \frac{1}{a_{11}a_{22} - a_{21}a_{12}}\begin{bmatrix} a_{22} & -a_{12} \\ -a_{21} & a_{11} \end{bmatrix}\left\{\begin{array}{c} b_1 \\ b_2 \end{array}\right\} \tag{11}$$

2.3 Disturbance rejection

This problem is more complex because the disturbance occurs only in a strip parallel to the x-axis of the rotor, see Fig. 2. The disturbances are limited to the thrust and rolling moment (pos. advancing side up) coefficients, the pitching moment is not affected, and hence $\Delta\Theta_C = 0$. Equation (9) is now set up for the disturbances only, Eq. (12). The control angle perturbations $\Delta\Theta_{75}$ and $\Delta\Theta_S$ act over the entire rotor disk, but within the area occupied by the propeller slipstream the integrals are more complicated because of the ΔU_T, ΔU_P terms. However, the problem can be split into two parts. First, the part of perturbation control angles on the entire rotor disk area in undisturbed flow; second, the part of the disturbance area only.

$$\left\{\begin{array}{c} \Delta C_T \\ \Delta C_{Mx} \end{array}\right\} = \frac{1}{2\pi}\int_0^{2\pi}\int_0^1\left\{\begin{array}{c} 1 \\ r\sin\psi \end{array}\right\}\Delta dC_T\,d\psi \overset{!}{=} \left\{\begin{array}{c} 0 \\ 0 \end{array}\right\} \tag{12}$$

For the first part, the differential lift only due to $\Delta\Theta$ is taken, see Eqs. (5) and (8), without the $\Delta\Theta_C$ term for the aforementioned reason, and defined by Eq. (13).

$$\Delta dC_T^{[1]} = \frac{\sigma C_{l\alpha}}{2}U_{T0}^2\Delta\Theta\,dr = \frac{\sigma C_{l\alpha}}{2}\left(r + \mu_0\sin\psi\right)^2\left(\Delta\Theta_{75} + \Delta\Theta_S\sin\psi\right)dr \tag{13}$$

Evaluation of the integrals results in Eq. (14), and the coefficients a_{ij} are the same as in Eq. (11):

$$\left\{\begin{array}{c} \Delta C_T^{[1]} \\ \Delta C_{Mx}^{[1]} \end{array}\right\} = \frac{\sigma C_{l\alpha}}{2}\left\{\begin{array}{c} \left(\frac{1}{3} + \frac{\mu_0^2}{2}\right)\Delta\Theta_{75} + \frac{\mu_0}{2}\Delta\Theta_S \\ \frac{\mu_0}{3}\Delta\Theta_{75} + \left(\frac{1}{8} + \frac{3\mu_0^2}{16}\right)\Delta\Theta_S \end{array}\right\} = \begin{bmatrix} a_{11} & a_{12} \\ a_{21} & a_{22} \end{bmatrix}\left\{\begin{array}{c} \Delta\Theta_{75} \\ \Delta\Theta_S \end{array}\right\} \tag{14}$$

The remaining part includes all contributions from perturbation velocities and thus is to be integrated only within the area covered by the slipstream, i.e. in the range from y_1 to y_2, see Fig. 2, which affects all lower and upper bounds of the integrals. Therein, the incremental lift due to the disturbances of the propeller slipstream and due to the control angle perturbations as given in Eq. (8), without the contribution of part [1], is denoted as part [2] given by Eq. (15). The third and fourth part represent solely the disturbance of the slipstream, combined with the undisturbed rotor's trim controls, part [3] in Eq. (16), and solely including perturbation velocity terms, part [4] in Eq. (17). The associated aerodynamic moment with respect to the hub center is, as before, $r\Delta dC_T^{[j]}, j = 2, 3, 4$. The radial and azimuthal bounds of the integrals are now limited by the width and position of the propeller slipstream within the disk, see Fig. 2. With $\mu = \mu_0 + \Delta\mu, c_\mu = 2\mu_0 + \Delta\mu$ and $\Delta_{\mu\lambda} = \mu_0\Delta\lambda + \lambda\Delta\mu$:

$$\Delta dC_T^{[2]} = \frac{\sigma C_{l\alpha}}{2}\left[\left(2U_{T0}\Delta U_T + \Delta U_T^2\right)\Delta\Theta\right]dr$$

$$= \frac{\sigma C_{l\alpha}}{2}\left[2\left(r + \mu_0\sin\psi\right)\Delta\mu\sin\psi + \Delta\mu^2\sin^2\psi\right]\left(\Delta\Theta_{75} + \Delta\Theta_S\sin\psi\right)dr$$

$$= \frac{\sigma C_{l\alpha}}{2}\Delta\mu\left[\Delta\Theta_{75}2\left(r\sin\psi + \mu\sin^2\psi\right) + \Delta\Theta_S 2\left(r\sin^2\psi + \mu\sin^3\psi\right)\right]dr$$

(15)

$$\Delta dC_T^{[3]} = \frac{\sigma C_{l\alpha}}{2}\left(2U_{T0}\Delta U_T + \Delta U_T^2\right)\Theta_0\,dr$$

$$= \frac{\sigma C_{l\alpha}}{2}\left[2\left(r + \mu_0\sin\psi\right)\Delta\mu\sin\psi + \Delta\mu^2\sin^2\psi\right]$$
$$\left[\Theta_{tw}(r - 0.75) + \Theta_{75} + \Theta_S\sin\psi\right]dr$$

(16)

$$= \frac{\sigma C_{l\alpha}}{2}\Delta\mu\left\{\Theta_{tw}\left[2\left(r^2 - 0.75r\right)\sin\psi + c_\mu(r - 0.75)\sin^2\psi\right]\right.$$
$$\left. + \Theta_{75}\left(2r\sin\psi + c_\mu\sin^2\psi\right) + \Theta_S\left(2r\sin^2\psi + c_\mu\sin^3\psi\right)\right\}dr$$

$$\Delta dC_T^{[4]} = -\frac{\sigma C_{l\alpha}}{2}\left[U_{T0}\Delta U_P + \Delta U_T U_{P0} + \Delta U_T\Delta U_P\right]dr$$

$$= -\frac{\sigma C_{l\alpha}}{2}\left[(r + \mu_0\sin\psi)\Delta\lambda + \lambda_0\Delta\mu\sin\psi + \Delta\lambda\Delta\mu\sin\psi\right]dr$$

(17)

$$= -\frac{\sigma C_{l\alpha}}{2}\left[\Delta\lambda r + \Delta_{\mu\lambda}\sin\psi\right]dr$$

Several cases must be identified. Consider the slipstream overlaps on the advancing side, with $y_2 \geq 1$ outside of it. When $y_1 \leq -1$, the entire rotor is within the propeller slipstream and the integral bounds are 0 to 2π for the azimuth and 0 to 1 for the radius as before (Case 0), with the solution for rotor controls as in Eqs. (10) and (11), replacing μ_0 by μ and λ_0 by λ. The difference to the undisturbed trim control angles then are the $\Delta\Theta_{75}, \Delta\Theta_S, \Delta\Theta_C$. But this means the helicopter rotor is smaller than the propeller diameter, which is unrealistic. Realistic cases will have a rotor diameter larger than the propeller slipstream width and five cases given in Table 2 can be identified.

Because the areas affected to the right and left of $x = 0$ are symmetric to the y-axis, see the differently shaded areas in Fig. 3 (a) and (b), the perturbation lift in the first and second quadrant is the same, and its moment with respect to the x-axis as well. The same holds true for the retreating side in the third and fourth quadrant of the disk. Therefore, the total perturbation thrust and rolling moment is twice the value of the first quadrant's (advancing side) or of the fourth quadrant's (retreating side) contribution. This reduces the number of regions to be computed. Due to this symmetry, no pitching moment can develop and, therefore, no lateral cyclic control angle is needed: $\Delta\Theta_C = 0$. All the upper and lower bounds of the different regions for all Cases 0 to V are listed in Table 3.

Exemplarily for Case II: the integral over the azimuth must be split into two regions as sketched in Fig. 3 (a): "Region 1" extends from $\psi_1 = \tan^{-1}\left(y_1/\sqrt{1 - y_1^2}\right)$ to $\psi_2 = \tan^{-1}\left(y_2/\sqrt{1 - y_2^2}\right)$ with radial range from $r_{low} = |y_1/\sin\psi|$ to $r_{up} = 1$. "Region 2" extends from ψ_2 to $\pi/2$ and the upper radial bound is $r_{up} = |y_2/\sin\psi|$. A position on the retreating side of the rotor disk, Case IV, is treated accordingly to that: "Region 3" from $-\pi/2$ to ψ_1 with radial range from $r_{low} = |y_2/\sin\psi|$ to $r_{up} = |y_1/\sin\psi|$ and "Region 1" from ψ_1 to ψ_2 with radial range from $r_{low} = |y_2/\sin\psi|$ to $r_{up} = 1$ as sketched in Fig. 3 (a). Case III, see Fig. 3 (b), includes the rotor center, thus $r_{low} = 0$ everywhere, and three regions must be computed:

Table 2 Case selection

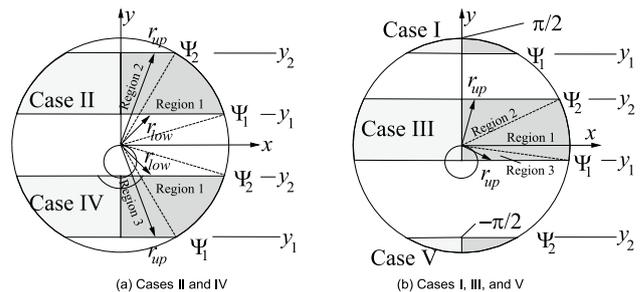| Case	Explanation: the slipstream…
0	Covers the entire rotor
I	Overlaps with the advancing edge of the rotor
II	Is within the advancing side of the rotor disk, see Fig. 3 (a), top
III	Overlaps with the rotor center, see Fig. 3 (b)
IV	Is within the retreating side of the rotor disk, see Fig. 3 (a), bottom
V	Overlaps with the retreating edge of the rotor

Fig. 3 Azimuthal and radial regions of integration for different cases **a** Cases II and IV. **b** Cases I, III, and V

Table 3 Radial and azimuthal integration bounds for all regions of all cases

Case	y_1	y_2	ψ_1	ψ_2	N_{reg}	Region	r_{low}	r_{up}	ψ_{beg}	ψ_{end}
0	≤ -1	≥ 1	n.a	n.a	1	1	0	1	$-\frac{\pi}{2}$	$\frac{\pi}{2}$
I	$\geq 0,$ < 1	≥ 1	$\tan^{-1}\frac{y_1}{\sqrt{1-y_1^2}}$	n.a	1	1	$\frac{y_1}{\sin\psi}$	1	ψ_1	$\frac{\pi}{2}$
II	$\geq 0,$ $< y_2$	$> y_1, < 1$	$\tan^{-1}\frac{y_1}{\sqrt{1-y_1^2}}$	$\tan^{-1}\frac{y_2}{\sqrt{1-y_2^2}}$	2	1	$\frac{y_1}{\sin\psi}$	1	ψ_1	ψ_2
						2	$\frac{y_1}{\sin\psi}$	$\frac{y_2}{\sin\psi}$	ψ_2	$\frac{\pi}{2}$
III	$< 0, > -1$	$> 0, < 1$	$\tan^{-1}\frac{y_1}{\sqrt{1-y_1^2}}$	$\tan^{-1}\frac{y_2}{\sqrt{1-y_2^2}}$	3	1	0	1	ψ_1	ψ_2
						2	0	$\frac{y_2}{\sin\psi}$	ψ_2	$\frac{\pi}{2}$
						3	0	$\frac{y_1}{\sin\psi}$	$-\frac{\pi}{2}$	ψ_1
IV	$< y_2,$ > -1	$\leq 0,$ $> y_1$	$\tan^{-1}\frac{y_1}{\sqrt{1-y_1^2}}$	$\tan^{-1}\frac{y_2}{\sqrt{1-y_2^2}}$	2	3	$\frac{y_2}{\sin\psi}$	$\frac{y_1}{\sin\psi}$	$-\frac{\pi}{2}$	ψ_1
						1	$\frac{y_2}{\sin\psi}$	1	ψ_1	ψ_2
V	≤ -1	$\leq 0,$ > -1	n.a	$\tan^{-1}\frac{y_2}{\sqrt{1-y_2^2}}$	1	1	$\frac{y_2}{\sin\psi}$	1	$-\frac{\pi}{2}$	ψ_2

"Region 3" from $-\pi/2$ to ψ_1 with $r_{up} = |y_1/\sin\psi|$, then "Region 1" from ψ_1 to ψ_2 with $r_{up} = 1$, finally "Region 2" from ψ_2 to $\pi/2$ with $r_{up} = |y_2/\sin\psi|$. Because the fractions $y_1/\sin\psi$ and $y_2/\sin\psi$ are always positive on the advancing and on the retreating side, there is no need to calculate the modulus, so it is omitted in Table 3.

The thrust and moment integrations of Eq. (12), due to the varying number of regions to be obeyed, become more tedious and must be set up as a sum of the N_{reg} various individual regions i_{reg} of the specific Case (0, I to V) considered, with $\Delta dC_T^{[j]}$ from Eqs. (15)–(17).

$$\begin{Bmatrix} \Delta C_T^{[j]} \\ \Delta C_{Mx}^{[j]} \end{Bmatrix} = \frac{1}{2\pi} \sum_{i_{reg}=1}^{N_{reg}} \int_{\psi_{beg}(i_{reg})}^{\psi_{end}(i_{reg})} \int_{r_{low}(i_{reg})}^{r_{up}(i_{reg})} \begin{Bmatrix} 1 \\ r\sin\psi \end{Bmatrix} 2\Delta dC_T^{[j]}\, d\psi; \quad j = 2,3,4$$

(18)

The evaluation of the inner integrals is simple as only $\int r^n dr = r^{n+1}/(n+1), n = 0,1,2,3$ are encountered, but the lower and upper bounds introduce powers $1/\sin^{n+1}\psi$ to the arguments of the outer integral. This results into $\int \sin^m\psi\, d\psi, m = -2, -1, \ldots, 4$ to be solved, with the solutions given next, without the trivial solution ψ for $m = 0$.

$$\int \sin^m\psi\, d\psi = \begin{cases} -\cot\psi & m = -2 \\ \ln\left|\tan\frac{\psi}{2}\right| & m = -1 \\ -\cos\psi & m = 1 \\ \frac{1}{2}\left(\psi - \frac{\sin 2\psi}{2}\right) & m = 2 \\ -\left(\cos\psi - \frac{\cos^3\psi}{3}\right) & m = 3 \\ \frac{1}{2}\left(\frac{3}{4}\psi - \frac{\sin 2\psi}{2} + \frac{\sin 4\psi}{16}\right) & m = 4 \end{cases}$$

(19)

Therefore, the solution of Eq. (18) poses no mathematical difficulty, but becomes quite lengthy with lots of terms. All contributions to the thrust and moment coefficients from Eqs. (14) and (18) with the $\Delta dC_T^{[j]}, j = 2,3,4$ from Eqs. (15) to (17) are put together for the disturbance rejection equations.

$$\begin{Bmatrix} \Delta C_T \\ \Delta C_{Mx} \end{Bmatrix} = \begin{bmatrix} a_{11} & a_{12} \\ a_{21} & a_{22} \end{bmatrix} \begin{Bmatrix} \Delta\Theta_{75} \\ \Delta\Theta_S \end{Bmatrix} + \begin{bmatrix} a_{11}^{[2]} & a_{12}^{[2]} \\ a_{21}^{[2]} & a_{22}^{[2]} \end{bmatrix} \begin{Bmatrix} \Delta\Theta_{75} \\ \Delta\Theta_S \end{Bmatrix} + \begin{bmatrix} b_{11}^{[3]} & b_{12}^{[3]} & b_{13}^{[3]} \\ b_{21}^{[3]} & b_{22}^{[3]} & b_{23}^{[3]} \end{bmatrix} \begin{Bmatrix} \Theta_{tw} \\ \Theta_{75} \\ \Theta_S \end{Bmatrix}$$
$$+ \begin{bmatrix} b_{14}^{[4]} & b_{15}^{[4]} \\ b_{24}^{[4]} & b_{25}^{[4]} \end{bmatrix} \begin{Bmatrix} \Delta\lambda \\ \Delta_{\mu\lambda} \end{Bmatrix} \stackrel{!}{=} \begin{Bmatrix} 0 \\ 0 \end{Bmatrix}$$

(20)

The first term on the right side is from Eq. (14) and represents the lift and moment of the perturbation control angles acting on the entire disk in the undisturbed flow and all other terms are evaluated only in the region occupied by the propeller slipstream. The second contains the contribution of the perturbation controls combined with the perturbations of the advance ratio. The third term represents the contribution of the undisturbed rotor's trim control angles combined with the perturbations of the advance ratio. Finally, the fourth term represents the contributions of the undisturbed advance ratio and inflow, combined with the perturbations of these. This set of linear algebraic equations is easily solved for the perturbation control angles required to mitigate the disturbance of the propeller slipstream.

$$\begin{bmatrix} a_{11} + a_{11}^{[2]} & a_{12} + a_{12}^{[2]} \\ a_{21} + a_{21}^{[2]} & a_{22} + a_{22}^{[2]} \end{bmatrix} \begin{Bmatrix} \Delta\Theta_{75} \\ \Delta\Theta_S \end{Bmatrix} = -\begin{bmatrix} b_{11}^{[3]} & b_{12}^{[3]} & b_{13}^{[3]} & b_{14}^{[4]} & b_{15}^{[4]} \\ b_{21}^{[3]} & b_{23}^{[3]} & b_{23}^{[3]} & b_{24}^{[4]} & b_{25}^{[4]} \end{bmatrix} \begin{Bmatrix} \Theta_{tw} \\ \Theta_{75} \\ \Theta_S \\ \Delta\lambda \\ \Delta_{\mu\lambda} \end{Bmatrix}$$

(21)

This can be expressed in matrix form; with $\vec{u}$ containing the vector of blade twist, the trim controls and the inflow and advance ratio perturbations on the right, and

as system matrix for the response to the control angles. By simple inversion of , the perturbation control angles required to reject the propeller slipstream perturbation are obtained.

$$\mathbf{A}\overrightarrow{\Delta\Theta} = \mathbf{B}\,\overrightarrow{u} \qquad \Rightarrow \qquad \overrightarrow{\Delta\Theta} = \mathbf{A}^{-1}\mathbf{B}\,\overrightarrow{u} \qquad (22)$$

with

$$\mathbf{A}^{-1} = \frac{1}{\det(\mathbf{A})}\begin{bmatrix} \left(a_{22} + a_{22}^{[2]}\right) & -\left(a_{12} + a_{12}^{[2]}\right) \\ -\left(a_{21} + a_{21}^{[2]}\right) & \left(a_{11} + a_{11}^{[2]}\right) \end{bmatrix} \qquad (23)$$

The power required by the rotor will also be affected by the propeller's slipstream disturbance and can be computed as well by blade element momentum theory, but this is not the subject of the current investigation with focus on rotor trim.

3 Results

3.1 Rotor trim in undisturbed air

A variation in the center position of the slipstream across the rotor disk requires solving the set of equations for all Cases I to V. Although this is straight forward algebra and not mathematically complicated, it is tedious and quite lengthy, therefore, not given here. All these derivations and results are given in the Supplement.

All terms of the perturbation are related to the strength of the additional velocity in the slipstream, $\Delta\mu_\infty$. Therefore, the control angles required for the disturbance rejection are divided by this parameter. The second influence stems from the width of the slipstream, i.e. the ratio of the radius of the contracted slipstream to the helicopter's rotor radius influenced by it, R_∞/R. For example, $\Delta\mu_\infty$ can be very large, but when the width of the slipstream approaches zero its influence on rotor aerodynamics becomes zero as well. Alternatively, even when the width of the slipstream is large relative to the rotor, its influence vanishes with $\Delta\mu_\infty$ approaching zero.

For a practical example, a configuration with the operational parameters as listed in Table 4 is used. The parameters are taken from a case investigated in Ref. [4] within the DLR project F(AI)^{2}R. The aircraft has the wing flaps deployed in a middle position. The basic trim of the helicopter rotor to its thrust coefficient and, for simplicity, to zero hub rolling and pitching moment coefficients is computed by using Eq. (11). The results for the blade pitch control angles are given in Table 5, together with the propeller velocities in the contracted slipstream, and its width ratio (related to the propeller radius and to the helicopter rotor radius).

In this example with a flight speed of $V_\infty = 65.7$ m/s as used in Fig. 1, the area affected by the propeller slipstream

is subjected to an increase in flight speed by Eq. (2) of $\Delta V_\infty = 27.4$ m/s, ca. 40%, and thus exceeds both the V_{max} and the V_{NE} of the helicopter locally by 26 and 11 m/s, respectively, but only over a fraction of the rotor disk. The advance ratio of the rotor is $\mu_0 = 0.3017$ and within the slipstream it is $\mu = 0.4272$. With data from Table 1 and Table 4, the slipstream contraction ratio Eq. (3) becomes $R_\infty/R_p = 0.923$ and hence $y_2 - y_1 = D_\infty/R = 0.448$. In maximum, the width $y_2 - y_1$ of the strip is subjected to the slipstream velocity within the helicopter rotor, which in this example amounts to 44.8% of the rotor radius, a significant amount. With Eq. (4) and data from Table 4, the flight speed ratio $\mu_\infty = 0.3084$ can be decomposed into its in-plane contribution, the advance ratio $\mu_0 = 0.3017$, and the inflow ratio normal to the disk, $\mu_{z0} = 0.0641$. The rotor thrust coefficient is approximately $C_T \approx 0.0099$ and for simplicity the steady hub moment coefficients may be required to be zero: $C_{Mx} = C_{My} = 0$.

3.2 Disturbance rejection

Using the operational data from Table 4, the results of rotor trim in undisturbed flow from Table 5 and the rotor blade pre-twist from Table 1, the additional control angles $\Delta\Theta$ can be computed that are required to reject the disturbance due to the slipstream on rotor thrust and hub moments. The individual contributions to the rotor thrust of the blade twist Θ_{tw}, trim control angles Θ_{75}, Θ_S, inflow ratio perturbation $\Delta\lambda$ and combined advance ratio / inflow ratio perturbation $\Delta_{\mu\lambda}$, represented by the elements $b_{1i}u_i$ of Eq. (21), are given in Fig. 4 (a) together with the total change in thrust $\Delta C_T/\sigma$. In Fig. 4 (b), the respective contributions $b_{2i}u_i$ of Eq. (21) to the rolling moment $\Delta C_{Mx}/\sigma$ and the total change as the sum of all contributions are shown.

In these figures, y_p represents the slipstream (= propeller) center position within the rotor lateral coordinate, with a value of $y_p = 1.0$ as the advancing side edge of the rotor disk (in this example, the right side of the rotor), 0.0 being the rotor center, and -1.0 the retreating side edge of the disk. The contributions of blade pretwist (solid line) are generally small and independent of the trim condition; therefore, it is not discussed here. For a slipstream position on the advancing side the lift caused by the slipstream in combination with the trim collective angle Θ_{75} (long dashed line) causes a large increase in lift due to the increased dynamic pressure while for a position on the retreating side a loss of lift is resulting, due to the loss of dynamic pressure. The moments related to Θ_{75} shown in Fig. 4 (b) are positive for either cases, because the arm of these lift perturbations to the rotor center is positive on the advancing side and negative on the retreating side.

The influence of the cyclic trim control angle Θ_S (medium dashed line) is less pronounced. Because the pitch angle

Table 4 Operational condition for a representative air-to-air refueling situation

Parameter	Symbol	Unit	Value
Height above sea level	h	m	2130
Temperature	T_∞	°C	1.16
Air density	ρ_∞	kg/m³	0.9933
Speed of sound	a_∞	m/s	332.6
Flight speed	V_∞	m/s	65.71
Flight Mach number	M_∞		0.1976
Aircraft mass	m_{airc}	T	130.0
Aircraft angle of attack	α_{airc}	deg	11.65
Glide ratio with flaps	ϵ		6.68[*]
Propeller thrust	T_p	kN	47.73
Rotational speed	Ω_p	rad/s	88.2
Blade tip speed	$(\Omega R)_p$	m/s	235.5
Tip Mach number	$M_{tip,p}$		0.708
Helicopter mass	m_{hel}	T	17.0
Rotor disk tilt angle	α_S	deg	− 12.0[*]
Rotational speed	Ω	rad/s	19.37
Blade tip speed	ΩR	m/s	213.1
Tip Mach number	M_{tip}		0.641
Flight speed ratio	μ_∞		0.3084
Rotor advance ratio	μ_0		0.3017
Rotor inflow ratio	μ_{z0}		0.0641

[*]estimated

due to Θ_S is negative on the advancing side, the increase in dynamic pressure there generates a negative lift as seen in Fig. 4 (a), while on the retreating side, the angle is positive, but the loss of dynamic pressure there also causes a loss of lift, yet less than on the advancing side. Therefore, the resulting associated rolling moments in Fig. 4 (b) are negative for slipstream positions on the advancing side, and positive for positions on the retreating side.

Table 5 Helicopter trim in undisturbed flow and propeller slipstream data

Parameter	Symbol	Unit	Value
Collective control angle	Θ_{75}	deg	12.31
Longitudinal cyclic control angle	Θ_S	deg	− 6.26
Lateral cyclic control angle	Θ_C	deg	0.0
Slipstream contraction ratio	R_∞/R_p		0.9228
Slipstream width ratio	$2R_\infty/R$		0.4480
Slipstream velocity	ΔV_∞	m/s	27.35
Slipstream velocity ratio	$\Delta\mu_\infty$		0.1283
Perturbation advance ratio	$\Delta\mu$		0.1255
Inflow ratio perturbation	$\Delta\lambda$		0.0218
Combined inflow and advance ratio perturbation	$\Delta_{\mu\lambda}$		0.0194

The fourth contribution to lift and moments stems from the perturbation inflow ratio $\Delta\lambda = \Delta\mu_z + \Delta\lambda_i$, all of them assumed as constant all over the area of the rotor disk occupied by the slipstream. For the negative disk tilt angle required for fast forward flight, the slipstream velocities increase the value of $\Delta\mu_z$, while the induced inflow ratio $\Delta\lambda_i$ is reduced due to the increased overall advance ratio. However, here $\Delta\mu_z$ dominates over $\Delta\lambda_i$. For all slipstream positions within the disk, this additional inflow ratio reduces the local angles of attack, therefore the lift generated, as seen in Fig. 4 (a), with maximum loss of lift for a center position. The respective rolling moment shown in Fig. 4 (b) is thus negative for slipstream positions on the advancing and positive for positions on the retreating side.

Finally, the mixed term $\Delta_{\mu\lambda} = \mu_0\Delta\lambda + \lambda\Delta\mu$ combining the perturbations of the advance ratio and the inflow ratio is discussed. Because all its elements are positive, $\Delta_{\mu\lambda}$ is positive as well. As shown in Fig. 4 (a), the perturbation lift generated by this term is negative on the advancing side. With the passage of the slipstream over the rotor center, it is quickly turning its sign to the same amount of now additional lift generation on the retreating side. Because the lift of this part is in opposite sign to the lift of the collective control angle, the resulting respective moments shown in Fig. 4 (b) are always negative, also opposing the moments due to the collective control angle.

The sum of all contributions then forms the total change of lift and rolling moment, indicated by the red curves in Fig. 4 (a) and (b). These perturbations have to be cancelled by perturbation control angles in collective and cyclic controls following Eq. (22) and the result is shown in Fig. 5.

For slipstream positions on the advancing side, the rotor lift is slightly reduced and the rolling moment is slightly negative due to the slipstream influence, as shown in Fig. 4. This can be opposed by a rather small amount of collective control angle $\Delta\Theta_{75}$ and a little more in the longitudinal cyclic control angle $\Delta\Theta_S$. Note that the latter—at this advance ratio—simultaneously increases the rolling moment and to a less extent the rotor lift. For slipstream positions on the retreating side, however, all individual lift contributions (except $\Delta_{\mu\lambda}$) lead to a rather large loss of lift—much more than for positions on the advancing side—and to a positive rolling moment, see Fig. 4. Because of the reduced dynamic pressure for such slipstream positions on the retreating side, both collective and cyclic control angles become less effective and rather large perturbation control angles are required for disturbance rejection.

Because the basic operating condition is already close to the limits of the flight envelope and rather large collective and cyclic control angles are applied for rotor trim, the additional angles required to keep the trim for slipstream interactions on the retreating side may cause the control system to run into the mechanical limits of the maximum
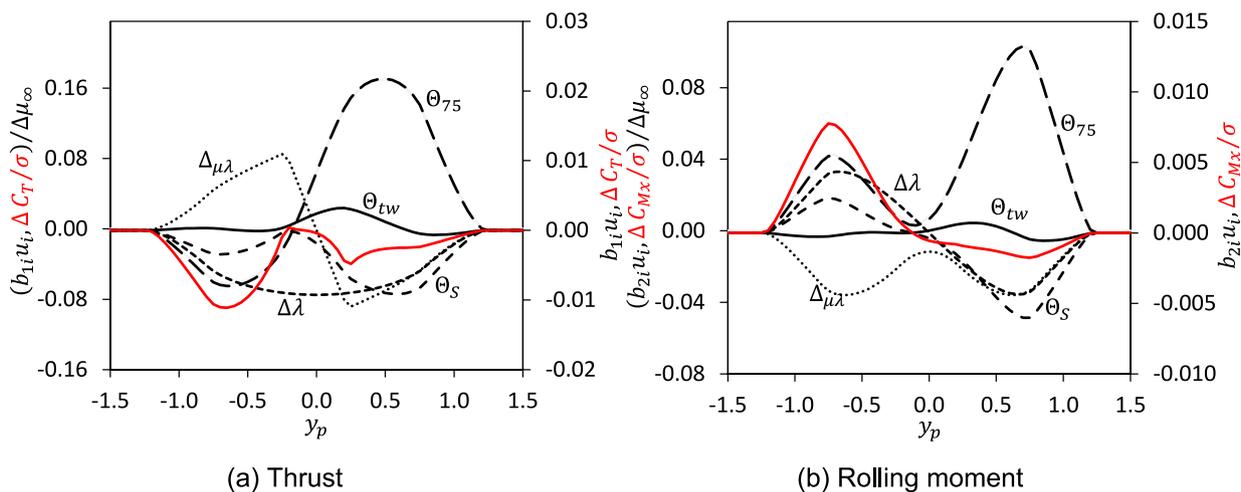
Fig. 4 Contributions to the perturbation thrust and rolling moment due to a propeller slipstream at varying lateral position. Operating conditions see Table 4, rotor trim controls from Table 5.

control angles. The smaller sensitivity to pilot controls for slipstream positions on the retreating side requires large control angles, i.e. pilot action, and therefore may lead to a higher workload for the pilots, in contrast to the increased sensitivity for slipstream positions on the advancing side.

To verify the analytical solution, the problem is also solved numerically based on 20 evenly spaced blade elements from root to tip and in 2 deg azimuth increments, i.e. with 180 steps per revolution. The comparison of the results is shown in Fig. 5 (b), and all details are represented by the numerical solution. The small differences of in maximum 0.06 deg in $\Delta\Theta_{75}$ and 0.09 deg in $\Delta\Theta_S$ can be attributed to the discretization error.

Fig. 5 Rotor controls required for propeller wake disturbance rejection

4 Parameter variations

The following sections include variations of the rotor shaft angle (representative for a variation in helicopter drag), the propeller diameter (and hence, the slipstream width to rotor radius ratio), the propeller slipstream velocity (equivalent to a variation of the propeller thrust), and the rotor thrust (representative for a variation in helicopter weight); all of them at constant flight speed. Their influence on rotor controls required for trim in undisturbed air is shown first (only needed in case of shaft angle and rotor thrust variation), and the rotor controls required for disturbance rejection are investigated. The results are computed by the analytical solution.

4.1 Shaft angle

When all other parameters are kept constant and only the rotor shaft angle is varied, each variation requires a rotor trim in undisturbed air first. Results for collective, longitudinal and lateral cyclic control angles are given in Fig. 6. The thick symbols denote the reference condition as investigated in the previous section. The results reflect textbook solutions: an essentially linear variation in the control angles is found. When approaching $\alpha_S = 0$ deg, less collective control angle is needed because of reduced rotor inflow, and the lateral aerodynamic lift imbalance generated by the collective control and rotor inflow is compensated by a smaller magnitude of the longitudinal cyclic control angle. The lateral control angle, due to zero rotor coning, remains zero throughout the variation.

Rotor controls required for propeller wake disturbance rejection relative to the trim controls in undisturbed air are shown in Fig. 7 (a) for the collective and in (b) for the
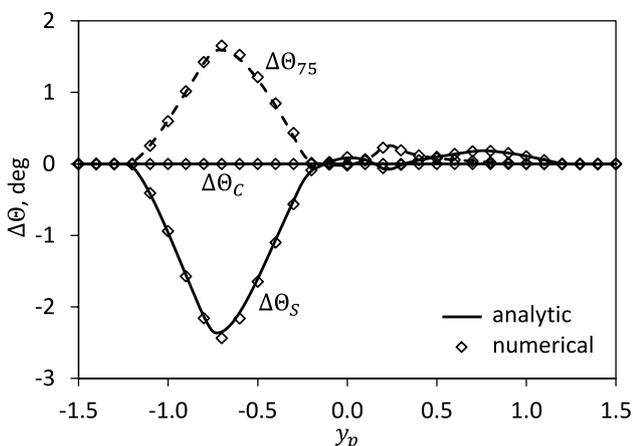
longitudinal control angle. The data of the reference condition are emphasized in bold. When approaching $\alpha_S = 0$ deg, the slipstream contribution to the inflow within the region occupied by it is diminishing, but the influence on the blade element tangential velocity and with it the section angle of attack as well as the dynamic pressure remains. Therefore, slipstream positions on the advancing side gain importance and require less collective control than in the reference condition, while the collective control becomes less sensitive for positions on the retreating side. Contrarily, when increasing the shaft tilt nose-down to -18 deg, the inflow contribution of the slipstream increases relative to the reference condition and more collective control is required on both advancing and retreating side slipstream positions.

Figure 7 (b) shows the associated variation in the longitudinal control angle, which balances the combined effects of collective control and slipstream velocity on the
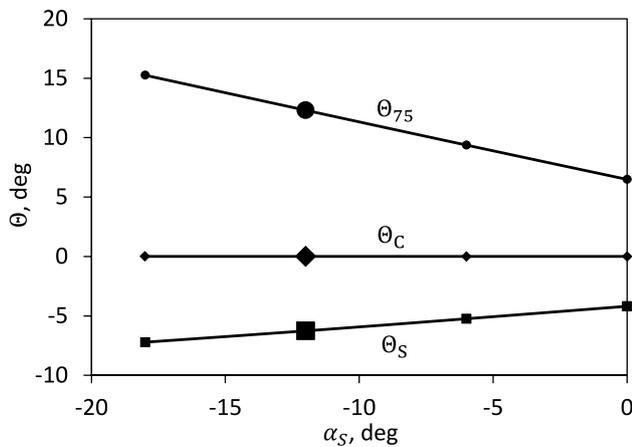
aerodynamic rolling moment. The magnitude becomes smaller when approaching zero deg shaft angle, and larger for more nose-down tilt of the rotor.

4.2 Slipstream diameter

Here, the rotor shaft angle is kept at the reference condition, the propeller slipstream velocity is maintained as well, but the propeller diameter and with it the contracted slipstream diameter ratio is varied to values of $D_\infty/R = 0.112, 0.224, 0.672, 1.35, 3.0$ and ∞ (25, 50, 150, 300, 570, ∞ percent) of the reference size (100% with $D_\infty/R = 0.448$). Infinity is equivalent to a flight speed of the rotor increased by the slipstream velocity. The rotor trim in undisturbed air is the same as that of the reference condition.

Results are shown in Fig. 8 (a) for the collective and in (b) for the longitudinal cyclic control angle. The smaller the propeller size, the smaller the area affected in the rotor by the propeller slipstream, and logically the smaller the control angles required to reject the disturbance. Asymptotically, the controls approach zero for a slipstream with zero width, because in that case, no disturbance is remaining. Contrarily, for increasing propeller diameter (and with it, increasing slipstream size), the required controls become larger in magnitude and also for a growing range of slipstream positions. In the case of an infinite slipstream width, the entire rotor is immersed in the slipstream velocity and the straight line represents the new rotor trim relative to the former reference condition. The rotor in this example is then operated at a total advance ratio of $\mu = \mu_0 + \Delta\mu$ with the values given in Tables 4 and 5. The significantly larger new advance ratio requires 2.4 deg more collective control angle and -2.96 deg more longitudinal control angle.
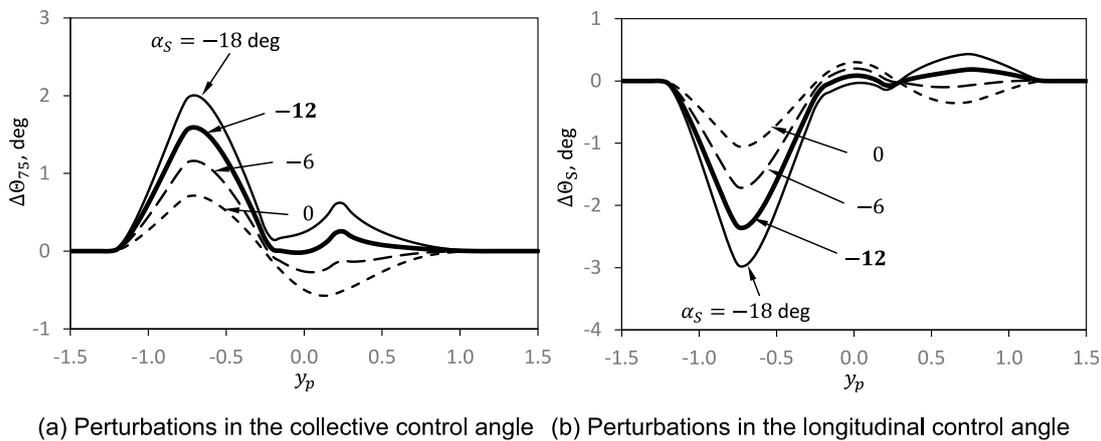

Fig. 6 Rotor shaft angle influence on rotor controls, trim in undisturbed air

(a) Perturbations in the collective control angle   (b) Perturbations in the longitudinal control angle

Fig. 7 Rotor controls required for propeller wake disturbance rejection for different rotor shaft angles

4.3 Slipstream velocity

Now, the propeller thrust is varied in a way such that the slipstream velocity ratio results in $\Delta\mu_\infty = 0.0367, 0.0697, 0.2265$ (25, 50, 180 percent) of the reference value (100%; $\Delta\mu_\infty = 0.1283$). Again, the rotor trim in undisturbed air is unchanged, as is the slipstream width. The results shown in Fig. 9 (a) and (b) for the collective and longitudinal control angles, respectively, represent the logical trend of diminishing control angles required with vanishing disturbance, and larger ones for increasing disturbance strength.

4.4 Rotor thrust

Finally, the impact of rotor thrust variations is investigated, while the rotor shaft angle is kept constant. Because a different thrust of the rotor requires a new trim in undisturbed air, this is performed prior to the disturbance rejection analysis. Trim results are given in Fig. 10 and the reference value is $C_T/\sigma = 0.0774$. The variation covers values of 0.0592, 0.0683, 0.0865 (76%, 88%, 112% of the reference value). To obtain increasing thrust, more collective control than for the reference thrust is needed, and for less thrust, vice versa. The lateral cyclic control angle is unaffected in this configuration without coning and constant inflow distribution, as before. The longitudinal cyclic control angle follows the collective. The more collective, the more longitudinal cyclic control magnitude is needed, and vice versa, which are textbook results that need no further explanation.

The differences to the undisturbed trim control angles of Fig. 10 are given in Fig. 11 with the slipstream acting in the rotor disk. As can be seen, the magnitude of collective and longitudinal control angles are very insensitive to the rotor thrust.

Changing the rotor thrust also changes its induced velocity, i.e., induced inflow ratio. This is covered by the rotor trim. Within the width of the slipstream in the rotor disk, the slipstream velocity itself also remains unchanged, but the change of rotor-induced velocities due to the higher advance ratio within the area covered by the slipstream changes differently compared to the reference condition. This difference is rather small, and consequently the variation in perturbation trim controls is rather small, too, and can hardly be distinguished. Therefore, the variation of rotor thrust can be judged as unimportant.

5 Conclusions

The analytical solution of a rotor in forward flight subjected to a laterally confined slipstream of a propeller ahead of it is presented by means of simple blade element momentum theory. It is a condition representative for air-to-air refueling of helicopters behind a tanker aircraft powered by large propellers. Results are verified by numerical analysis which is also used to perform a sensitivity study with respect to variation in rotor angle of attack, propeller radius, propeller thrust and rotor thrust. The following conclusions can be drawn:

1. The propeller slipstream comes along with rather high additional downstream velocities, increasing the local advance ratio by ca. 40%, which may locally exceed the V_{NE} of the helicopter.
2. Due to the large nose-down tilt of the helicopter rotor in fast forward flight the propeller slipstream locally increases the inflow normal to the rotor disk as well,
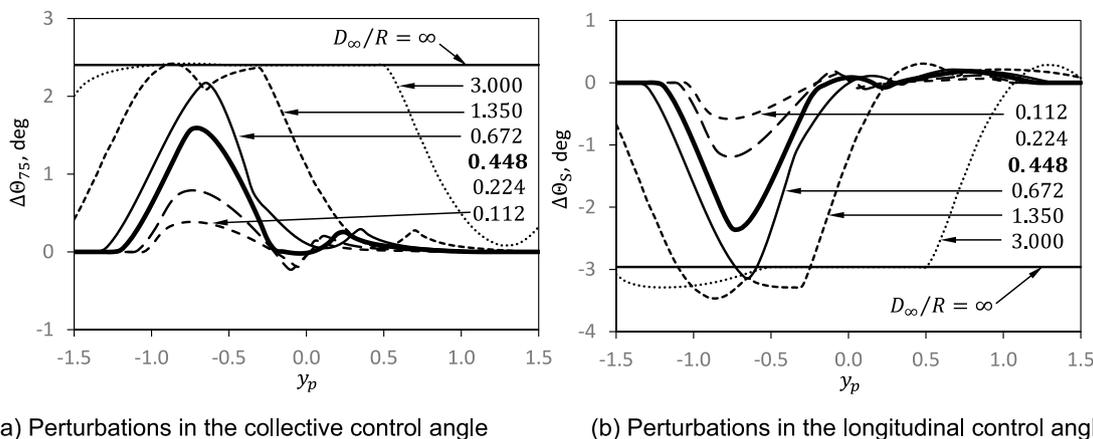

(a) Perturbations in the collective control angle (b) Perturbations in the longitudinal control angle

Fig. 8 Rotor controls required for propeller wake disturbance rejection for different slipstream diameters

(a) Perturbations in the collective control angle

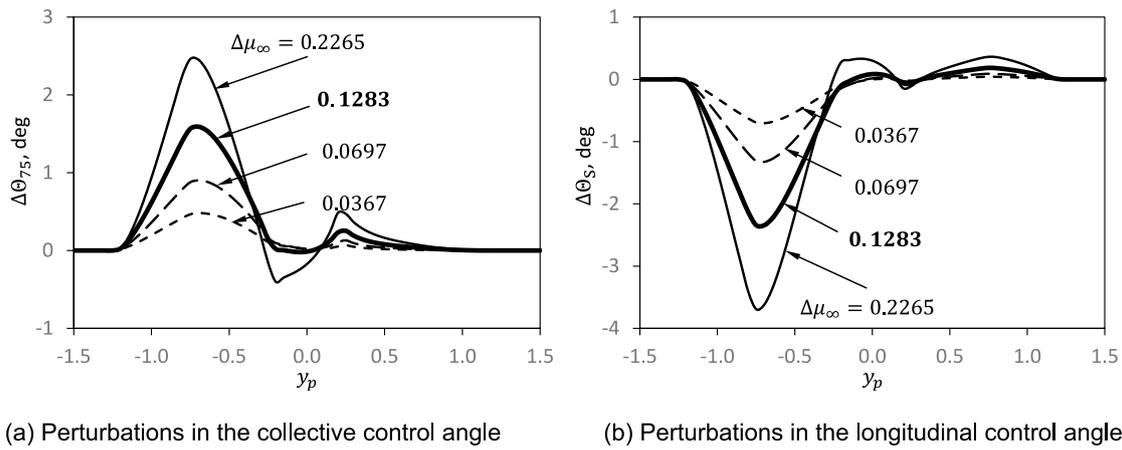(b) Perturbations in the longitudinal control angle

Fig. 9 Rotor controls required for propeller wake disturbance rejection for different slipstream velocities
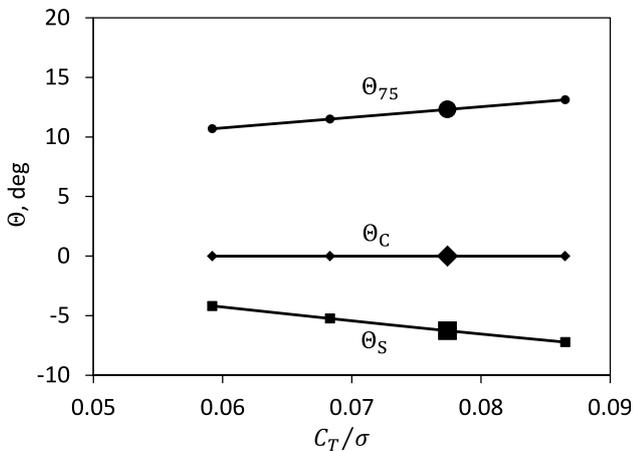

Fig. 10 Rotor thrust influence on rotor controls, trim in undisturbed air, $\alpha_S = -12$ deg

simultaneously reducing the rotor thrust-induced velocity due to the increased advance ratio.

3. The pilot controls to reject the propeller slipstream disturbances of rotor trim are small for slipstream positions on the advancing side, due to high sensitivity of local lift to pilot controls in the high dynamic pressure area.

4. The pilot controls to reject the propeller slipstream disturbances of rotor trim are large for slipstream positions on the retreating side, due to low sensitivity of local lift to pilot controls in the reduced dynamic pressure area. The total rotor controls may then reach mechanical limits.

5. The difference in control sensitivity will lead to high pilot workload, especially for slipstream positions on the retreating side.

6. Therefore, it appears advised to approach the refueling position with the advancing side of the rotor near the

(a) Perturbations in the collective control angle

(b) Perturbations in the longitudinal control angle
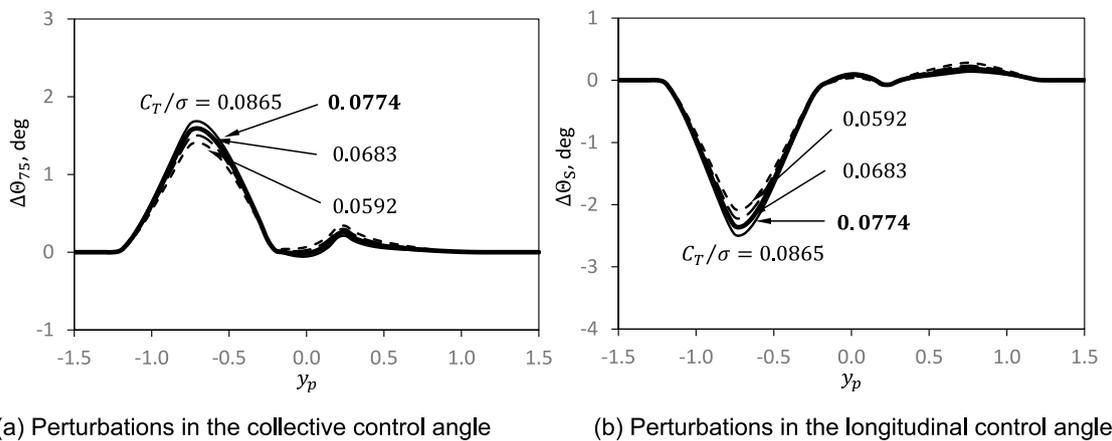
Fig. 11 Rotor controls required for propeller wake disturbance rejection for different rotor thrust.

propeller slipstream, and not with the retreating side near to it.

7. Rotor shaft angle variations have a significant impact on perturbation controls. A pitch-up reduces their magnitude and a pitch-down increases them.

8. The propeller diameter to rotor radius ratio, i.e. the slipstream width, has a very important influence on the controls required for disturbance rejection, as a growing ratio implies a growing affected area of the rotor.

9. Propeller thrust—and with it the slipstream velocity—has a strong impact on trim controls. The larger the velocity, the larger the control angles required.

10. Rotor thrust variations change the rotor trim, but the control angles required to mitigate the propeller slipstream disturbance are only marginally affected.

Future activities are devoted to investigate the changes of thrust and moment when no retrim is performed, the inclusion of rotor blade flapping in response to that, and the control angles required for retrim to zero flapping, while the blade coning will vary due to the slipstream acting on the rotor.

Declarations

References

1. Dunn, H.P.: The USAF CH-3C helicopter V/STOL in-flight refueling program and its operational uses and implications. 22nd Annual Forum and Technology Display of the Am. Helicopter Soc. proceedings, Washington, D.C. (1966)

2. Kashawlic, B.E., Irwin, J.G.III, Bender, J.S., Schwerke, M.: MH-47G DAFCS helicopter aerial refueling control laws. 67th Annual Forum and Technology Display of the Am. Helicopter Soc. proceedings, Virginia Beach, VA (2011)

3. Thomas, P.R., Bhandari, U., Bullock, S., Richardson, T.S., du Bois, J.L.: Advances in air to air refuelling. Prog. Aerosp. Sci. **71**, 14–35 (2014). https://doi.org/10.1016/j.paerosci.2014.07.001

4. Schmidt, S.O., Jones, M., Löchert, P.: Evaluation of a real-time simulation environment for helicopter air-to-air refuelling investigations. Aeronautical. J. **127**(1311), 754–772 (2023). https://doi.org/10.1017/aer.2022.106

5. Löchert, P., Schmidt, S.O., Jann, T., Jones, M.: Consideration of tanker's wake flow for helicopter air-to-air refueling. AIAA Aviat. For., Virtual (2021). https://doi.org/10.2514/6.2021-2561

6. Osborne, T.: A400M helicopter aerial refueling now a research project. Aviation week & space technology, **177**, New York (2015)

7. van der Wall, B.G., van der Wall, L.B.: Analytical estimate of rotor controls required for a straight vortex disturbance rejection. J. Am. Helicopter Soc. **62**(1), 1–4 (2017). https://doi.org/10.4050/JAHS.62.015001

8. van der Wall, B.G.: Analytical estimate of rotor controls required for a propeller wake disturbance rejection. J. Am. Helicopter Soc. **69**(4), 1–6 (2024). https://doi.org/10.4050/JAHS.69.045011

9. Leishman, J.G.: Principles of Helicopter Aerodynamics. Cambridge University Press, New York, NY, 2000, Chapters 2.3 and 2.4.

10. Stepniewski, W.Z., Keys, C.N.: Rotary-Wing Aerodynamics. Dover Publications, Inc., Mineola, NY, 1984, Chapter 3.2.